FULL PAPER

Tailored gas adsorption properties of electrospun carbon nanofibers for gas separation and storage

Ansgar Kretzschmar*[a, b], Victor Selmert[a, b], Henning Weinrich[a], Hans Kungl[a], Hermann Tempel[a], Rüdiger-A. Eichel[a, b]

[a] Forschungszentrum Jülich GmbH
Institute of Energy and Climate Research – Fundamental Electrochemistry (IEK-9)
52425 Jülich
Germany
[b] RWTH Aachen University
Institute of Physical Chemistry
52056 Aachen
Germany

Supporting information for this article is given via a link at the end of the document.

Abstract: In this work electrospun Polyacrylonitrile (PAN) derived carbon nanofibers (CNFs) are investigated with respect to their gas adsorption properties. By employing CO_2 adsorption measurements it is shown that adsorption capacity and selectivity of the fibers may be tailored by the applied carbonization temperature. General carbon nanofiber pore properties are identified by Ar adsorption measurements, whereas CO_2 adsorption measurements provide information about the ultramicroporosity, adsorption energies and the adsorption capacities. Ideal adsorbed solution theory (IAST) selectivities at practically relevant conditions are determined by the evaluation of single component data for N_2 and CO_2. Especially for low carbonization temperatures the CNFs exhibit a very good low pressure adsorption performance and excellent CO_2/N_2 IAST selectivities of 350 at 20 mbar and 132 at 1 bar, which are attributed to a molecular sieve effect in very narrow slit pores. These IAST selectivities represent some of the highest values for carbon materials reported in literature so far and the highest IAST selectivities for as prepared, non-post-treated carbon ever.

Introduction

The scientific significance and public perception of the anthropogenic climate change is increasing significantly[1], as the fraction of CO_2 in the atmosphere has reached 407 ppm and is still growing. To attenuate the devastating effects of climate change, CO_2 emissions have to be reduced by any means. Two feasible ways to do so are to avoid the consumption of fossil fuels such as crude oil and natural gas and to capture and store CO_2 whenever possible. Although technologically and economically challenging, the latter may have benefits besides the reduction of CO_2 emissions. Once separated from other gases, CO_2 can chemically be transformed into value-added organic compounds such as methanol[2] or ethylene[3]. For this, electrochemical CO_2 reduction is particularly attractive due to its versatility[4] and the possibility to combine both CO_2 capture and utilization in one process. By transforming CO_2 into synthetic fuels or raw organic chemicals, a closed carbon cycle can be established leading to a CO_2 neutral economy.

Aiming at efficient CO_2 adsorption materials[5], an excessive number of different materials have been investigated, including metal-organic frameworks (MOFs)[6-8], zeolites[9-12], carbons[13-17], polymers[18] and functionalized silica[19]. Among these materials, carbons offer several advantages over zeolites and MOFs, since they are widely abundant, cheap, easy to prepare and comparatively insensitive towards contaminants such as water[5,20,21]. Moreover, in contrast to polymers, carbons are mostly electrically conductive[20], which enables an application as current collector in CO_2 electrolyzers as well. However, two aspects, which are missing with respect to present carbon materials, are a decent adsorption capacity as well as CO_2 selectivity at low pressure, which are significantly better for tailor-made MOFs, yet[5,21].

According to the numerous advantages a large variety of carbons has been investigated in search of improved CO_2 adsorption properties[15–17]. Many of these were biomass based, for example carbons which have been prepared from soy bean dreg[22], coconut[23], palm shell[24], bamboo[25] and many more. Biomass based carbons are fairly easy to prepare and cheap. However, tailoring their properties is demanding since the chemical composition and structural information, i.e., the pore system, is fixed by the precursor[15]. In contrast, carbons may also be synthesized from polymers, which provide a higher controllability of the chemical properties. This includes carbons obtained from melamine[26] or urea[27] based resins as well as carbonized Polypyrrole[28], Polyindole[29], Polyvinylidene fluoride (PVDF)[30] and Polyacrylonitrile (PAN)[31–33].

Aiming for a maximum CO_2 adsorption capacity and selectivity, two main approaches are available for carbon materials. Firstly, nitrogen functional groups can be introduced into the carbon matrix[34], as a high nitrogen content is favorable due to acid-base interactions between the adsorbent and CO_2: The number and nature of nitrogen based functional groups is usually adjusted by nitrogen containing precursors or subsequent functionalization of the prepared carbons. However, the impact of certain nitrogen groups on the CO_2 adsorption properties is still a matter of debate debate. While Li et al. consider pyrrolic groups most important for CO_2 adsorption[35], Kim et al. found a larger influence for pyridinic N-groups[33].

Secondly, the physical surface area may be increased by processes such as KOH etching or CO_2 activation in order to

increase the bare number of interaction sites[17]. Shen et al.[36] used KOH to activate commercial PAN fibers, which had a BET area of 0.24 m²/g. By KOH activation, the BET area was enlarged to 2231.24 m²/g, which increased the CO_2 capacity by a factor of ten to 4.5 mmol/g[36].

Besides the adsorption capacity, the selectivity is a second most important property, especially for practical applications. For instance, increasing the CO_2/N_2 selectivity of a typical material (CO_2 adsorption capacity = 3 mmol/g) from 50 to 100, can mitigate the cost for CO_2 capture from flue gas by 20%, i.e., from 35 to 28 USD/t[37].

For a high selectivity a narrow pore system rather than a high specific surface area is required to achieve a molecular sieve effect[21]. Moreover, the selectivity can further be enhanced by the introduction of nitrogen functionalities, which may contribute to a high selectivity due to selective interactions with CO_2 as well[21].

As a matter of fact, PAN derived carbons have been under investigation for CO_2 adsorption before and have mostly been obtained from bulk polymer[38] [39], wet spinning[31,35,36] or electrospinning[33]. However, most of these carbons were post-treated by various activation processes in order to achieve enhanced CO_2 adsorption properties. Thus, surprisingly little information is available on CO_2 adsorption on unmodified PAN derived carbon.

In this work, unmodified, electrospun, PAN derived carbon nanofibers (CNFs) are investigated as adsorbent for CO_2, aiming for a deeper understanding of the adsorption processes on polymer-based carbons. PAN derived CNFs are easy to prepare, even on a large scale and contain a significant amount of nitrogen functionalities, if an appropriate carbonization temperature is applied[40]. In electrospinning, a PAN polymer solution is spun in a controlled atmosphere using a high voltage electric field for the preparation of a carbon mat consisting of non-woven fibers. Afterwards, the PAN polymer chains are stabilized and crosslinked in air and carbonized in Argon, yielding carbon fibers in the sub micrometer range, i.e. carbon nanofibers, which feature a very high surface area[41]. Using this carbon material it is shown that the elemental composition and the pore properties of the as prepared CNFs are closely adjustable by the carbonization temperature and allow for an excellent low pressure adsorption capacity and selectivity towards CO_2. With this, the approach to prepare a highly selective carbon material proposed in this paper particularly abstains from excessive post-treatment keeping the synthesis procedure simple and, therefore, as cost-efficient and scalable as possible. As a result, we report a maximum CO_2 adsorption capacity of 1.5 mmol/g at 100 mbar and 2.8 mmol/g at 1 bar. Moreover, by tailoring the ultramicropore system (micropores < 0.7 nm)[42] it is possible to achieve an IAST selectivity of 350 at a low pressure of 20 mbar and 132 at 1 bar. Both values are very close to typical results for MOFs, among the highest values for carbon materials reported so far, and the highest value for unmodified carbons.

Results and Discussion

Fiber morphology, structure and chemistry

Upon electrospinning and carbonization at different temperatures ranging from 600 °C to 1100 °C carbon nanofiber (CNF) mats were prepared from a 10 wt% Polyacrylonitrile (PAN) solution as described in the experimental section. As a result, in the SEM images in Figure 1a-d it can be seen that the non-woven fibers show an even surface and do not exhibit any preferred orientation for all carbonization temperatures. The fiber diameters are rather uniform and decrease only slightly from 250 nm to 220 nm within the investigated carbonization temperature range. Moreover, the TEM images in Figure 1e and f reveal a slightly ordered carbon structure, which shows an increased surface roughness for an increasing carbonization temperature. A detailed in situ TEM analysis under vacuum for the effect of the carbonization temperature on the CNFs has been published elsewhere[43].

To analyze the chemical composition of the CNFs, an elemental analysis by the CHNO method was performed. The results of this analysis are shown in Table 1. It can be observed that the carbon content of the CNFs rises continuously for an increasing carbonization temperature from 600 °C to 1100 °C with a larger step from 77.6 wt% (900 °C) to 91.5 wt% (1000 °C). Simultaneously, the nitrogen content of the carbonized fibers decreases almost linearly from 23 wt% to 7 wt%. This correlation fairly matches the expectations based on literature, where 17 wt% nitrogen for 700 °C[44] and 5.8 wt% nitrogen for 1000 °C were reported[45] for carbonized PAN. In contrast to carbon and nitrogen, the oxygen content remains almost constant between 10 and 12 wt% in a temperature range from 600 °C to 900 °C, indicating a higher thermal stability of the remaining oxygen-containing functional groups. Above 900 °C the oxygen content

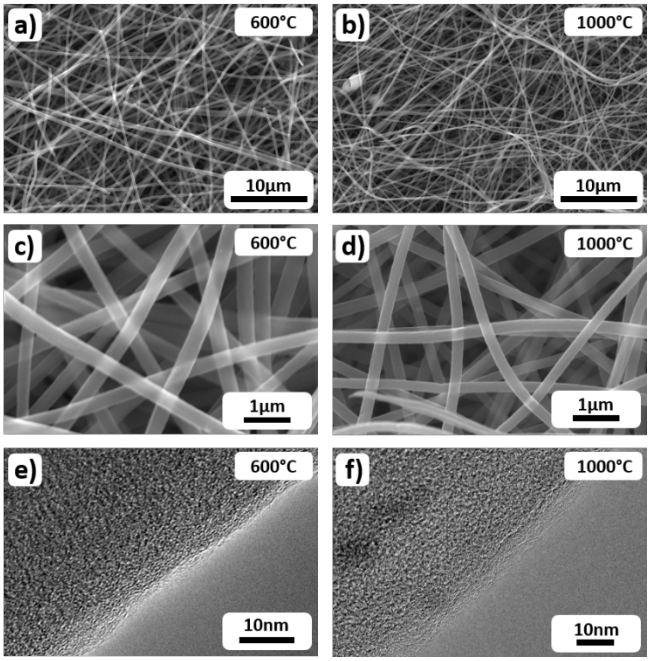

Figure 1: SEM (a-d) and TEM (e, f) images for some of the electrospun, PAN derived carbon nanofibers. Image a, c, and e display those fibers, which were carbonized at 600 °C. Images b, d, and f display the fibers, which were carbonized at 1000 °C.

decreases to 0.8 wt% for a carbonization temperature of 1100 °C. It is expected, that the majority of the oxygen groups present in the crosslinked fibers already decomposed and released oxygen as water at lower temperatures of 300 °C to 400 °C[45]. Furthermore, the hydrogen content is decreasing as well from 2.7 wt% to 0.4 wt%, indicating the progress of carbonization. In fact, at higher temperatures C-H bonds are thermally destroyed and crosslinking processes between carbon atoms take place[46].

Table 1: Elemental composition of the investigated carbon nanofibers as determined by CHNO analysis.

Carbonization Temperature	C [wt%]	N [wt%]	O [wt%]	H [wt%]
250 °C	52.2	22.6	24.1	2.7
600 °C	63.5	23.0	11.8	2.1
700 °C	67.9	19.9	11.1	1.8
800 °C	72.6	16.2	10.6	1.4
900 °C	77.6	11.6	9.5	1.2
1000 °C	91.5	7.1	3.1	0.4
1100 °C	95.8	3.7	0.8	0.5

In addition to the elemental analysis, XPS measurements were performed to characterize the surface composition and the functional groups of the individual fiber mats (for spectra and integration see Figures S2 and S3). Moreover, XPS also yields data with respect to the elemental composition, which are shown in Table 2. Comparing the data from the CHNO method and XPS, it can generally be observed that the individual results show a similar trend regarding the carbon and the nitrogen content. Being aware that comparing the exact numbers is not possible as XPS data is given in at% and CHNO data in wt%, the difference is small for light elements with similar atomic mass. However, the XPS data shows higher absolute values for carbon (76.5 to 95.1 at%) and lower absolute values for nitrogen (19.7 to 3.1 at%) and oxygen (3.8 to 1.8 at%). In addition, the sudden jump in the carbon content between the samples carbonized at 900 °C and 1000 °C is less pronounced for the XPS results as compared to the findings obtained by the CHNO method. In contrast to the results provided by the elemental combustion analysis (CHNO), the surface oxygen fraction determined by XPS is far lower and does not exceed 4 at%. Furthermore, the oxygen content does not show any trend depending on the carbonization temperature. This suggests that most of the oxygen, which was detected by the CHNO method, is trapped inside the fibers and is not accessible to XPS as this technique is surface sensitive only, limited to a penetration depth of a few nanometers[47] and also depends on the incident angle[48]. However, the difference between elemental analysis and XPS results can also be explained by the experimental procedure as the sample might contain adsorbed CO_2 or O_2 during the elemental analysis, whereas XPS is measured in ultrahigh vacuum. Furthermore, the measurement procedure for the determination of oxygen in the elemental analysis is only indirect (see experimental details), which could cause deviations.

Table 2: Elemental composition of the investigated carbon nanofibers as determined by XPS analysis.

Carbonization Temperature	C [at%]	N [at%]	O [at%]
600 °C	76.5	19.7	3.8
700 °C	80.4	16.8	2.8
800 °C	84.1	13.7	2.2
900 °C	86.6	11.0	2.4
1000 °C	92.6	4.3	3.1
1100 °C	95.1	3.1	1.8

Relative Error: ±15%

Besides the elemental composition, XPS measurements also provide information about the functional groups on the material surface. Especially nitrogen functional groups are of interest for CO_2 adsorption due to their basic nature[20,27,49] and their positive influence on weak hydrogen bonding interactions between CO_2 and hydrogen on the carbon surface[22]. Accordingly, the fractions of different nitrogen groups were evaluated depending on the applied carbonization temperature. As a result, Figure 2a depicts the XPS data normalized to the nitrogen peak area, while Figure 2b displays the same data multiplied by the total nitrogen content from Table 2, which provides the overall contribution of the nitrogen functional groups to the atomic surface composition. In Figure 2a, it can be observed that quaternary and pyridinic groups are the dominant species. In contrast, pyrrolic nitrogen as the third potentially important species is almost absent. When carbonizing at a comparatively low temperature of 600 °C, the number of

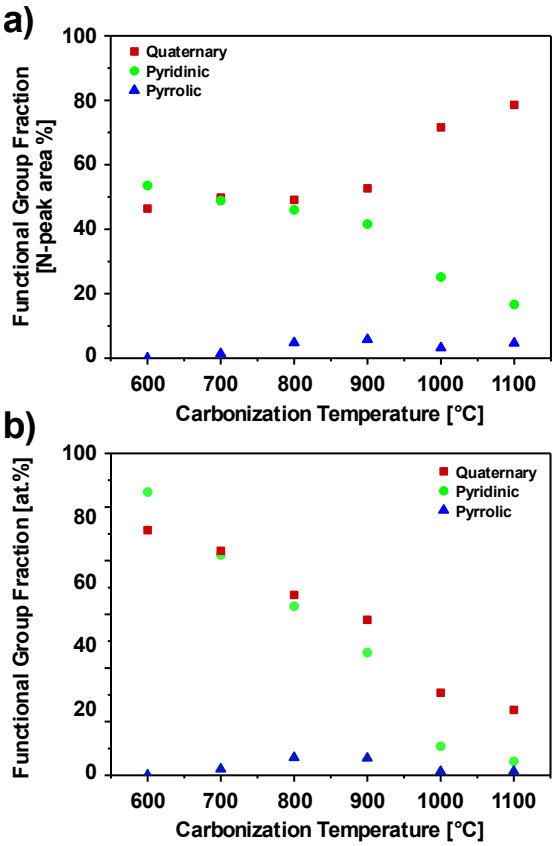

Figure 2: Results of the XPS analysis for electrospun, PAN derived carbon nanofibers carbonized at 600 °C to 1100 °C (for spectra and integration see Figures S2 and S3). (a) Functional surface group fraction normalized to nitrogen peak area. (b) Total fraction of surface atoms.

quaternary and pyridinic groups is almost equal, with a small advantage for pyridinic groups. However, for an increasing carbonization temperature, the fraction of quaternary in comparison to pyridinic groups increases, leading to a ratio of roughly 4:1 at 1100 °C. This can be explained by the fact that pyridinic nitrogen in carbonized PAN is transformed into quaternary nitrogen at high temperatures[50]. At the same time, the fraction of pyrrolic groups increases for increasing carbonization temperatures from 600 °C to 800 °C and remains - besides a small variation - constant and always below 5% beyond a carbonization temperature of 800 °C.

Taking a look at the fraction of nitrogen moieties in the total number of surface atoms in Figure 2b, it is obvious that – even though quaternary groups become more dominant – the absolute number of both quaternary and pyridinic groups continuously decreases from about 10 at% to below 2 at% for an increasing carbonization temperature. A possible reason is the decomposition of functional groups towards N_2, HCN and NH_3[50,51]. Furthermore, the number of pyrrolic moieties shows a maximum at a carbonization temperature of 800 °C and 900 °C, however their fraction as compared to the total number of surface atoms remains below 1 at% and does therefore most probably not play a significant role in CO_2 adsorption.

Ar adsorption, surface area and pore structure

Besides functional groups, the pore system of a material is considered as an important factor for CO_2 adsorption[49], since a larger surface area increases the number of potential adsorption sites. Furthermore, narrow pores are highly beneficial with respect to low pressure adsorption, as the adsorption potentials of opposing pore walls overlap[42,52]. To investigate the pore structure of the CNFs, static Argon adsorption measurements were performed at 87 K. The resulting isotherms are shown in Figure 3. For clarity, the results for the samples carbonized at 600 °C and 700 °C, and 800 °C to 1100 °C are shown separately in Figure 3a and b, and can be explained as follows. Upon carbonizing at 600 °C and 700 °C, the samples exhibit a type I isotherm[42], which is typical for microporous adsorbents. However, both isotherms are not in equilibrium as the desorption branches do not meet the adsorption branch at low relative pressures again, even though the isotherms were measured with the highest technically possible equilibration parameters. This pseudo-irreversibility of the Argon adsorption implies a kinetic hindrance, which is known to occur when ultramicropores smaller than 0.45 nm are present[53]. Comparing the isotherms, both show a similar total adsorbed amount of Ar of 4 mmol/g at ambient pressure (1000 mbar). The only significant difference between the two samples is the slope of the isotherm at relative pressures below 0.1. Here, the slope of the sample carbonized at 700 °C is much steeper, indicating narrower micropores or a higher adsorption energy, respectively.

In contrast to the underequilibrated isotherms of the samples carbonized at 600 °C and 700 °C, the samples carbonized at higher temperatures of 800 °C and above exhibit a well equilibrated type II isotherm without any hysteresis (Figure 3b), which is expected for non-porous samples or at least for samples

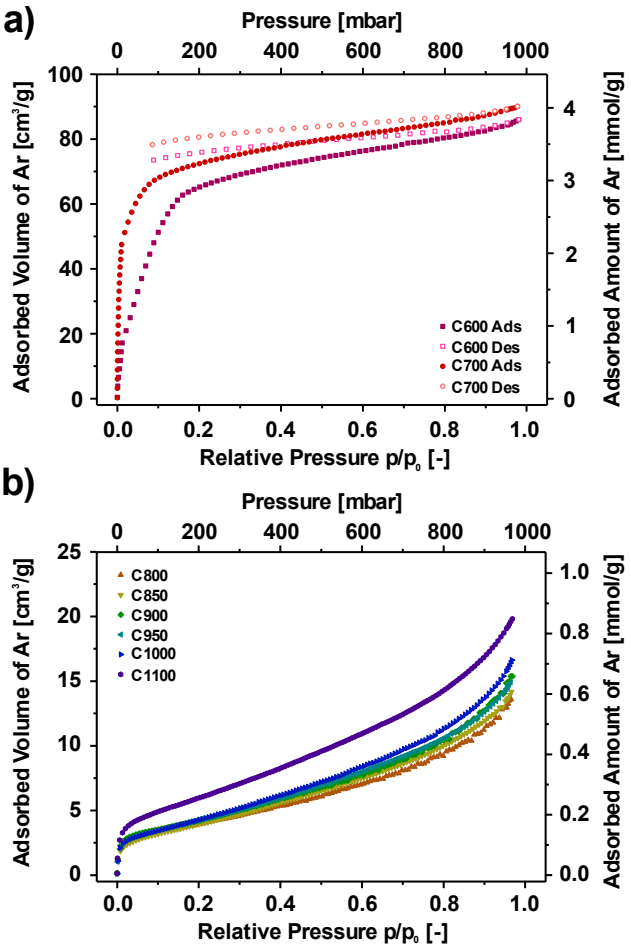

Figure 3: Ar adsorption isotherms for electrospun, PAN derived carbon nanofibers at 87 K. (a) Samples carbonized at 600 °C and 700 °C (C600 and C700) (b) Samples carbonized at 800 °C to 1100 °C (C800 — C1100). (In (b) the desorption branches are not shown for clarity, but can be found in Figure S4.).

that do not exhibit pores accessible to Ar. Furthermore, while the shape remains very similar for all samples, the overall adsorbed amount of Ar at 1000 mbar slightly increases from 0.6 to 0.9 mmol/g, which is most probably due to a slightly decreasing fiber diameter for an increasing carbonization temperature.

From the Ar adsorption isotherms BET areas were calculated and listed in Table 3. The samples carbonized at 600 °C and 700 °C exhibit BET areas of roughly 250 m²/g, which is comparatively high as these samples have not been activated by any additional reactant. Nevertheless, the value is low compared to chemically activated carbons, which easily exceed values of 1500 m²/g[31,36,38,39]. However, the results given for both samples should only be considered as rough estimates, since the recorded isotherms were not fully equilibrated. In contrast the samples carbonized at 800 °C to 1100 °C exhibit surface areas of about 15 m²/g, which is close to the expected value of 9 m²/g for non-porous fibers with a diameter of 200 nm. Overall, the surface areas show a slight trend to higher values for increasing carbonization temperatures as observed for the adsorbed gas volumes at ambient pressure.

Table 3: BET-data of the investigated carbon nanofibers (CNFs).

Carbonization Temperature	BET area [m²/g]	Carbonization Temperature	BET area [m²/g]
600 °C	259 *	900 °C	14.6
700 °C	249 *	925 °C	15.0
800 °C	13.4	950 °C	14.3
825 °C	12.4	975 °C	16.0
850 °C	13.1	1000 °C	14.8
875 °C	13.2	1100 °C	20.0

*underequilibrated isotherm

CO_2 adsorption and micropore structure

In addition to Ar adsorption measurements, CO_2 adsorption measurements were performed in order to study potential ultramicroporosity and general CO_2 adsorption properties of the CNFs. The CO_2 adsorption isotherms shown in Figure 4a were obtained at 273 K. (For clarity reasons, desorption branches as well as the results for the samples carbonized at 825 °C, 875 °C, 925 °C and 975 °C are not shown here, but can be found in Figure S6). Furthermore, Figure 4b shows the respective cumulative pore size distributions, which were obtained from the isotherms shown in Figure 4a.

In Figure 4a it can be observed that the individual CO_2 adsorption isotherms show marked changes in shape depending on the applied carbonization temperature. The samples carbonized at 600 °C to 850 °C show a steep increase of the adsorbed amount of CO_2 at low pressures, leading to 0.85 mmol/g at pressures as low as 25 mbar and 1.3 mmol/g at 75 mbar for 600 °C, which is a remarkable, since practically relevant result for carbon. In fact, an excellent low pressure performance is a key requirement for gas separation applications, e.g., CO_2 separation from flue gas with a low relative pressure of 8-13% for CO_2. (Please note: Unlike the Ar measurements, the samples carbonized at 600 °C and 700 °C were evaluated in equilibration due to the higher measurement temperature used for CO_2 adsorption[54]) At higher pressures, the isotherm slope for the sample carbonized at 600 °C decreases and results in a final amount of 2.7 mmol/g at 1 bar. In contrast to this, the sample carbonized at 900 °C shows a smaller initial slope of the CO_2 adsorption isotherm, but only a slightly reduced amount of adsorbed CO_2 of 2.4 mmol/g at 1 bar. At higher carbonization temperatures of 950 °C to 1100 °C the isotherms tend to become almost linear and the total adsorbed amount of CO_2 at 1 bar remains below 1.0 mmol/g. Furthermore, the adsorption kinetics for those samples which were carbonized between 950 °C to 1100 °C appear to become slower, since the difference between adsorption and desorption branch increases with higher carbonization temperatures (see Figure S6).

For an improved overview over the individual adsorption properties, the adsorbed amounts of CO_2 at certain pressure levels are given in Table S2 in comparison with some commercial carbons. Taking a look at a pressure of 50 mbar, it is obvious that the adsorbed amount of CO_2 for the sample carbonized at 600 °C is more than 50 times higher than that for the sample carbonized at 1000 °C. However, at ambient pressure, the amount of adsorbed CO_2 is only about 5 times higher. Nevertheless, in contrast to the commercial carbons chosen for comparison, samples carbonized at a temperature between 600 °C and 875 °C show an excellent low pressure adsorption performance,

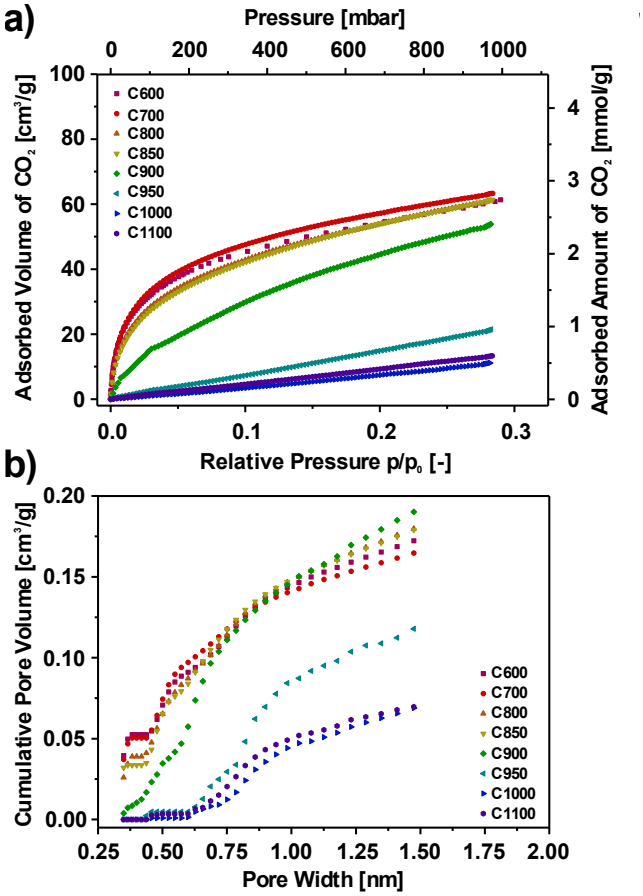

Figure 4: CO_2 adsorption properties for electrospun, PAN derived carbon nanofibers at 273 K carbonized at 600 °C to 1100 °C (C600 to C1100). (a) CO_2 adsorption isotherms (desorption branches not shown for clarity, see Figure S6). (b) Cumulative pore size distributions obtained by Monte-Carlo- (MC) calculations.

regardless of their comparatively low BET area. Black Pearls 2000® for example, possess a BET area of more than 1500 m²/g and adsorb 4.3 mmol/g CO_2 at ambient pressure, but their CO_2 uptake at 50 mbar is only about half of the amount for the samples carbonized at 600 °C to 875 °C. Furthermore, SuperP® as a nonporous carbon and graphene platelets with a medium scaled BET area of 250 m²/g also do not reach the adsorbed amounts of the investigated CNFs either, neither at low pressures nor at ambient pressure. Thus, the electrospun CNFs offer superior adsorption properties for CO_2 at low pressures in comparison to other carbons (see also Table S1), which favors an application in separating CO_2 from gas mixtures with low CO_2 concentrations.

In order to elucidate the origin of the superior adsorption properties, pore size distributions were derived from the individual CO_2 isotherms using standard Monte Carlo-calculations. As a result, the cumulative pore size distributions are shown in Figure 4b. Therein, it attracts attention that the samples carbonized at 600 °C to 850 °C appear to exhibit a significant amount of pores, which are smaller than the calculation limit of 0.35 nm. The latter is indicated by the fact that the cumulative pore volume curves do not start at 0 cm³/g, but slightly above at 0.05 cm³/g.

Overall, the pore volume of ultramicropores smaller than 0.40 nm decreases with increasing carbonization temperatures. Moreover, larger ultramicropores are present as well, reaching a total volume

of 0.1 cm³/g for the samples carbonized at 600 °C to 850 °C. In contrast to this, at a carbonization temperature higher than 950 °C the samples do not contain a significant measurable specific ultramicropore volume anymore, but still show some supermicroporosity (0.7 nm to 2.0 nm)[42].

As a matter of fact, the slit pore width of 0.35 nm, which was observed for the samples carbonized at 600 °C to 850 °C, is very close to the carbon layer distance in graphitic (0.3354 nm) or turbostratic carbon (0.34 nm)[55], which implies that the observed porosity in this range can be attributed to interlayer spaces of the carbon. In addition, the observed width range of the ultramicropores does not only lie close to the graphite layer distance, but matches the kinetic diameters of technically relevant gases, too. In fact, CO_2 possesses a kinetic diameter of 0.330 nm[56], while N_2 and Ar are slightly larger (0.364 nm[56] and 0.340 nm[54], respectively). Therefore, a molecular sieve effect appears to be a reasonable explanation for the excellent CO_2 adsorption capability compared to Ar.

An overview over the individual pore volume and other textural properties such as the micropore surface area S_{micro} obtained by MC (Monte Carlo) and DR (Dubinin-Radushkevich) calculations are given in Table 4 in comparison to commercial carbon materials.

Table 4: Textural properties (micropore surface area S_{micro}, cumulative pore volume at different thresholds) and adsorption energy of the investigated carbon nanofibers (CNFs) derived from CO_2 adsorption experiments on electrospun, PAN derived carbon nanofibers using Monte Carlo (MC) simulations and Dubinin Radushkevich (DR) calculations.

Carbonization Temperature	S_{micro} (MC)	$V_{<0,4\ nm}$ (MC)	$V_{>0,4\ nm}$ (MC)	V_{ges} (MC)	S_{micro} (DR)	V_{ges} (DR)	E_{ads} (DR)
	[m²/g]	[cm³/g]	[cm³/g]	[cm³/g]	[m²/g]	[cm³/g]	[kJ/mol]
600 °C	626	0.053	0.119	0.172	453	0.170	36.0
700 °C	618	0.051	0.114	0.165	484	0.182	34.9
800 °C	615	0.039	0.141	0.180	465	0.175	32.8
825 °C	599	0.039	0.133	0.172	460	0.173	32.9
850 °C	610	0.034	0.145	0.179	468	0.176	32.2
875 °C	656	0.035	0.156	0.191	519	0.195	31.9
900 °C	551	0.011	0.179	0.190	422	0.158	26.6
925 °C	318	0.004	0.132	0.136	160	0.060	23.2
950 °C	274	0	0.118	0.118	146	0.055	22.5
975 °C	160	0	0.071	0.071	90	0.034	21.7
1000 °C	151	0	0.069	0.069	95	0.036	20.3
1100 °C	165	0	0.070	0.070	104	0.039	21.9
SuperP®,[1]	299	0	0.134	0.134	212	0.080	19.4
Graphene Platelets[2] 300 m²/g	321	0.004	0.126	0.130	244	0.092	23.8
Black Pearls 2000®[3]	1173	0.007	0.470	0.477	936	0.351	23.0

[1] (Imerys); [2] (Aldrich); [3] (Cabot);

Evaluating the results in Table 4, it can be seen that for a carbonization temperature of 600 °C to 900 °C the carbon fibers exhibit micropore surface areas of roughly 600 m²/g (MC), which decreases to about 150 m²/g for a carbonization temperature of 1000 °C and above. The results derived by DR support the MC calculated values. However, the DR values are about 25% lower, which is suggested to be due to limitations of the DR-equation regarding the heterogeneity of surface chemistry or texture[57]. Furthermore, it attracts attention that even samples with a very low BET area of 15 m²/g show a significant micropore surface area of more than 600 m²/g (e.g. at 800 °C), which is, again, a hint that the ultramicroporosity of these samples is not accessible to Ar. Similar to the trend of the micropore surface area, the overall pore volume (MC) shows a drop from 0.190 cm³/g (900 °C) to 0.07 cm³/g (1000 °C), which is far less significant than the drop in the adsorbed amount of CO_2 at low pressures mentioned above. However, this trend complies better with the overall adsorbed amounts of CO_2 at 1 bar, which was found to be five times higher for a carbonization temperature of 600 °C than for 1000 °C. This observation can be explained by the fact that larger pores get filled at higher pressures only. The DR derived values for the micropore volume are comparable to those obtained by the MC-method. Interestingly, the drop in pore volume at 900 °C is sharper (0.195 cm³/g (875 °C) to 0.06 cm³/g (925 °C)) and slightly shifted towards lower carbonization temperatures when determined by DR, although both data sets were derived from the same raw data.

Comparing the results for the CNFs in Table 4 with commercially available carbons, it can be seen that Black Pearls 2000® exhibit a micropore surface area and a micropore volume which are twice as high as compared to the sample carbonized at 600 °C. The latter is in very good agreement with the doubled CO_2 loading at ambient pressure. On the other hand, SuperP® and Graphene Platelets show lower values, which corresponds to their CO_2 adsorption capacity at 1 bar as well.

Beyond micropore surface area and micropore volume, the DR-method allows to obtain adsorption energies for CO_2, which are given in Table 4 as well. For a carbonization temperature of 600 °C, the adsorption energy equals 36.0 kJ/mol and constantly decreases for an increasing carbonization temperature to 31.9 kJ/mol for the sample carbonized at 875 °C. Above 875 °C, the adsorption energy drops to 23.2 kJ/mol for 925 °C and remains fairly constant at about 20 kJ/mol for higher carbonization temperatures. For a further investigation, the isosteric heats of adsorption have been calculated as well. The heats of adsorption are shown in dependence of the carbonization temperature and CO_2 loading in Figure S8. For the samples carbonized from 600 °C to 800 °C the isosteric heats of adsorption are about 40 kJ/mol for a low amount of CO_2 and 25 kJ/mol for high CO_2 loadings. With carbonization temperature of 1000 °C and 1100 °C the isosteric heat falls to 10 kJ/mol and 5 kJ/mol, respectively. An increase in adsorption energy can be caused either by a stronger chemical interaction between functional groups or by an overlap of pore wall potentials in narrow pores. However, since the number of functional groups and the number of ultramicropores are increasing with lower carbonization temperatures, a clear separation of both effects is not possible.

Relating Ar and CO_2 adsorption measurements with each other, it is possible to calculate a surface affinity towards CO_2, dividing the adsorbed amount of CO_2 by the BET area. Evaluating the surface affinities towards CO_2, in can clearly be observed in

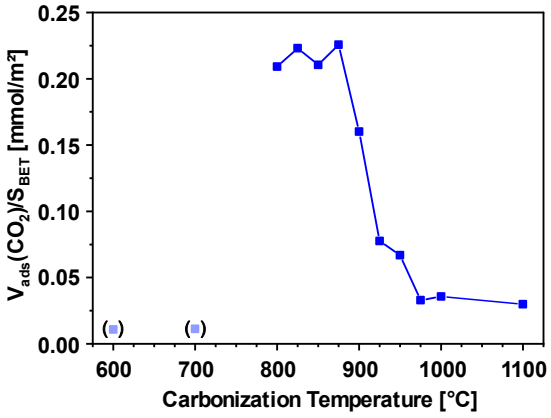

Figure 5: Ratio of adsorbed CO_2 vs. BET area (Ar) for electrospun, PAN derived carbon nanofibers depending on the carbonization temperature. (Data points in parentheses were obtained from underequilibrated isotherms.)

Figure 5 that CO_2 adsorption is highly favored within a carbonization temperature range of 800 °C to 900 °C. For these samples, the calculated surface affinities reach extremely high values of 0.2 mmol/m² and drop by one order of magnitude for a carbonization temperature of 975 °C and above, due to the significantly lower CO_2 adsorption capacity. For the samples carbonized at 600 °C to 700 °C the surface affinities are lower than 0.03 mmol/m², due to the higher accessible surface areas, which were, however, obtained from underequilibrated isotherms. Comparing the results in Figure 5 with literature, it is clear that the investigated CNFs feature remarkable properties. In fact, most carbons suggested for CO_2 adsorption show significantly lower values for the surface affinity and are typically below 0.005 mmol/m², due to the very high BET areas of the corresponding materials (Table S1). Taking the very narrow pore widths into account, the circumstance of an extraordinary surface affinity implies that the superior adsorption properties at low pressures and the very high selectivity towards CO_2 can be attributed to a molecular sieve effect. For a carbonization temperature of 600 °C and 700 °C, the narrowest micropores are accessible for both Ar and CO_2 molecules. Upon carbonizing between 800 °C and 875 °C, larger Ar atoms cannot penetrate the shrinking pores anymore, while CO_2 adsorption is still possible. Furthermore, upon further increase of the carbonization temperature, the micropores become too narrow to allow any of both CO_2 or Ar adsorption and the adsorption capacity decreases drastically. To substantiate the interpretation that a molecular sieve effect is a major driver of the observed adsorption behavior of Ar and CO_2, additional measurements of commercial zeolite molecular sieves with defined pore structure have been conducted. These measurements along with a short interpretation are shown in Figure S7.

Microporosity vs. surface functionality

Beyond microporosity, surface functionality is a second main factor influencing the CO_2 adsorption capacity of carbon materials[34], which can explain an increase in adsorption energy and surface affinity. Therefore, it will be discussed in competition with the effect of pore shrinkage in the following section. To do so, Figure 6a displays the micropore volume for pores narrower than 0.4 nm for all samples as given in Table 5. With this, Figure 6a

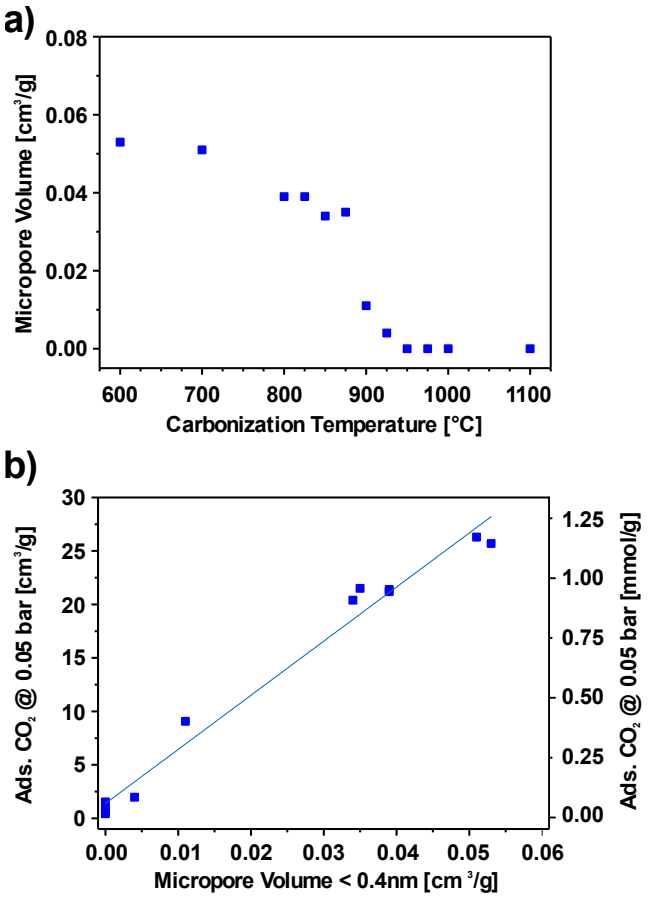

Figure 6: CO_2 adsorption properties at 273 K of electrospun, PAN derived carbon nanofibers carbonized at 600 °C to 1100 °C (C600 to C1100). (a) Impact of the carbonization temperature on the available micropore volume. (b) Relation between the micropore volume < 0.4 nm and the CO_2 adsorption properties at 0.05 bar.

reveals that the ultramicropore volume behaves similarly to the carbonization temperature-dependent surface affinity shown in Figure 5. For samples carbonized at 600 °C and 700 °C, the ultramicropore volume < 0.4 nm equals 0.05 cm³/g, while samples carbonized at 800 °C to 875 °C exhibit 0.04 cm³/g. Then, within a carbonization temperature range of only 100 °C, the micropore volume drops to 0 cm³/g for a carbonization temperature of 950 °C and beyond.

Furthermore, Figure 6b correlates the adsorbed amount of CO_2 at 50 mbar to the micropore volume smaller than 0.4 nm. Based on this plot, it can be concluded that the ultramicropore volume < 0.4 nm is a major driver for the adsorbed amount of CO_2 at 50 mbar. In fact, while a sample with an ultramicropore volume < 0.4 nm of 0 cm³/g adsorbs almost no CO_2, a sample with an ultramicropore volume < 0.4 nm of 0.05 cm³/g leads to 1.1 mmol/g of adsorbed CO_2 at 50 mbar already. The correlation between ultramicropore volume < 0.4 nm and adsorbed amount of CO_2 is almost linear. This observation is a strong hint, that at the given pressure of 50 mbar the ultramicropores are mainly responsible for the adsorption of CO_2, rather than the open surface, which is in accordance with results previously described in literature[58,59,60,61].

In order to study the correlation between nitrogen functional groups and the CO_2 uptake, the adsorbed amount of CO_2 at 50

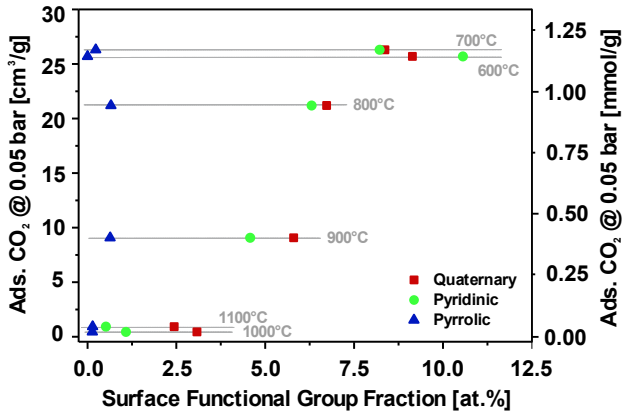

Figure 7: Influence of the nitrogen functional groups on the CO_2 adsorption capacity on electrospun, PAN derived carbon nanofibers at 0.05 bar.

mbar is plotted as a function of the surface functional group fraction of nitrogen as determined by XPS in Figure 7.

From Figure 7 it can be deducted, that there is a restrained correlation between pyridinic and quaternary groups and the adsorbed amount of CO_2. It appears that in a carbonization temperature range between 700 °C and 1000 °C both groups facilitate CO_2 adsorption. This is confirmed by the correlation of the nitrogen content determined by elemental analysis (Table 1), since the adsorbed amount of CO_2 is higher for the samples with a higher nitrogen content. Nevertheless, the correlation between adsorbed amount of CO_2 at 50 mbar and the nitrogen functional groups is less clear than the correlation between the adsorbed amount of CO_2 and the ultramicropore volume. In contrast to pyridinic and quaternary moieties, the amount of pyrrolic nitrogen is too small to show a significant effect towards CO_2 adsorption and no clear trend is visible. Similar results for the relation between CO_2 adsorption and nitrogen content have been reported by Zhang et al. for Polyaniline based carbons[58]. They described a positive influence of nitrogen on CO_2 adsorption, however with a significant scattering of data points.

In general, it is difficult to distinguish between the effect of microporosity and nitrogen surface groups on the CO_2 adsorption performance. Both parameters change continuously over the studied range of carbonization temperatures, thus, the influence of both might overlap and result in misleading correlations although previous studies found a synergetic effect of microporosity and N-doping[62]. In addition, the influence of microporosity and functional groups cannot be discussed independently, since it is not possible to reduce the nitrogen content without influencing the microporosity for the same polymer and same preparation procedure, respectively. As a reason, we assume that nitrogen acts as a structure disturbing heteroatom, whose number is reduced for an increasing carbonization temperature, resulting in less disturbance and, therefore, shrinkage of the carbon layer distance, i.e., narrower micropores.

All in all, combining both micropore and surface group analysis it can be deduced, that the influence of ultramicropores appears to be more significant than the impact of the nitrogen moieties. In fact, depending the actual carbonization temperature, it appears that slit pores with a variable width occur in between the carbon layers and govern the gas adsorption, which is schematically depicted in Figure 8. The samples carbonized at 600 °C and 700 °C can adsorb both CO_2 and Ar in rather high amounts in between the carbon layers (Figure 8e). However, the adsorption of Ar is extremely slow, which indicates that the pore width is very close to the limit that is accessible to Ar atoms, which exhibit a higher kinetic diameter than CO_2. For carbonization temperatures of 800 °C to 875 °C the carbon layer distances become too small to be penetrated by Ar, but can still adsorb significant amounts of CO_2, leading to an excellent surface affinity towards CO_2 (Figure 8f). When the CNFs are carbonized at even higher temperatures (900 °C to 1100 °C), the carbon layer coherence becomes too strong and even CO_2 cannot be adsorbed in between the carbon layers anymore (Figure 8g). Moreover, the narrowness of the carbon layer slit pores also leads to an excellent low pressure adsorption capability due to the overlap of pore wall potentials. The shrinkage of ultramicropore width is further supported by the fact that the pseudo irreversibility due to kinetic restrictions of CO_2 adsorption which is visible in CO_2 sorption isotherms (Figure S6) increases with the carbonization temperature. If a stronger interaction between functional groups and CO2 molecules was responsible for the pseudo irreversibility, the relation would be inverse.

Since the kinetic diameters of many technically relevant gases are in the range of slit pore width and since this carbon layer distance can be adjusted by choosing an appropriate carbonization temperature, it appears possible to tailor the material for many gas separation applications.

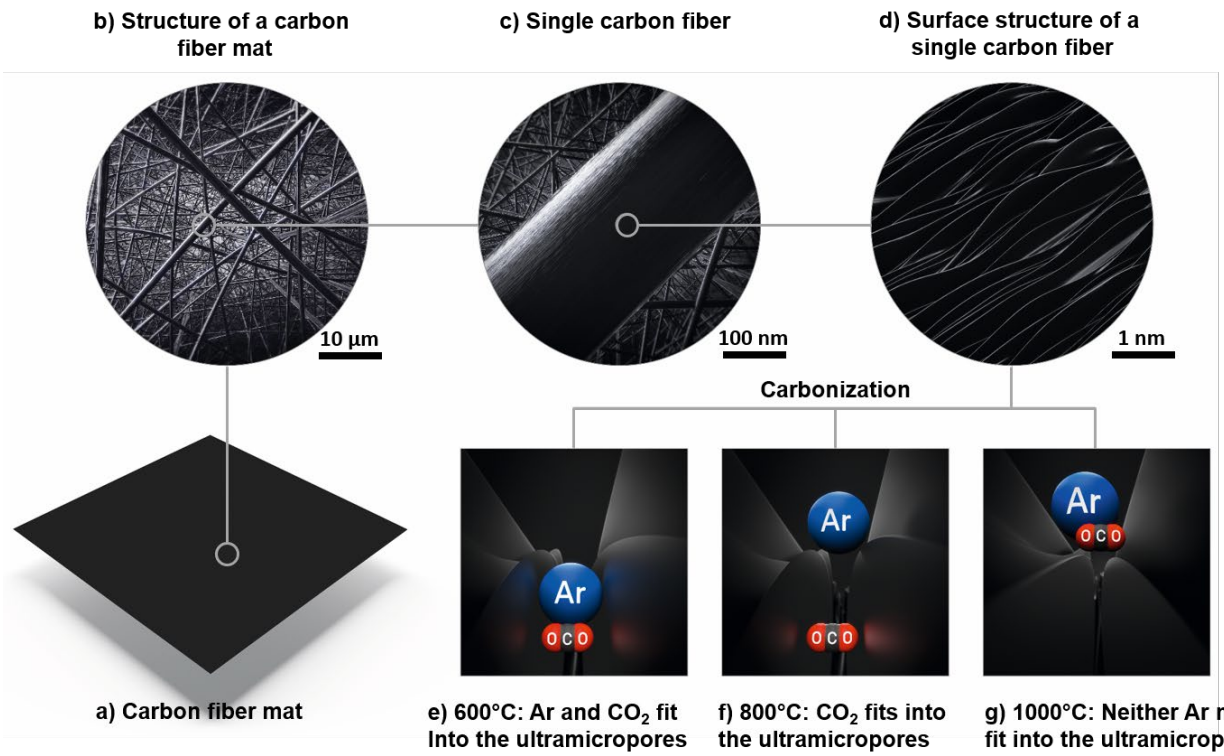

Figure 8: schematic overview of the Ar and CO_2 adsorption properties of CNFs carbonized at 600, 800 and 1000 °C. Schematic for Ar and CO_2 adsorption on electrospun, PAN derived carbon nanofibers carbonized at various temperatures ranging from 600 °C to 1100 °C. a) Schematic of an as-prepared, electrospun carbon fiber mat. b) Zoom into the carbon fiber mat showing randomly oriented carbon fibers. c) Zoom into the carbon fiber mat showing a single, as-prepared carbon fiber that features a homogeneous and smooth surface. d) Detailed view onto a single carbon fiber, depicting individual carbon layers, which act as slit pores with a varying slit pore width tailored by the applied carbonization temperature. e-g) Schematic explanation of the excellent CO_2 adsorption on the investigated carbon nanofibers. Due to a decreasing carbon layer distance, the adsorption of individual gas molecules is prevented by size exclusion, i.e., by a molecular sieve effect. e) Both Ar and CO_2 fit into the ultramicropores in between the carbon layers. f) Ar is excluded from adsorption within the slit pores due to a decreasing pore width for a carbonization at 800 °C. g) Both Ar and CO_2 are excluded from ultramicropore adsorption due to a further decrease in ultramicropore width.

IAST selectivity calculations

A very common application for CO_2 adsorbents is the separation of CO_2 from flue gas, which contains 8-13 % CO_2 and 71-73 % N_2. In order to evaluate the performance of the CNFs with respect to this application, additional gas adsorption measurements with N_2 were performed at 273 K. The adsorption isotherms of N_2 and CO_2 were simulated using a Tóth model (Table S3), which provides an affinity constant for the interaction between adsorptive and adsorbent. The affinity constant is much lower for N_2 adsorption than for CO_2 adsorption, indicating a high selectivity towards CO_2. Furthermore, the affinity constant for CO_2 decreases with higher carbonization temperatures, which is a hint that the selectivity may decrease as well.

Combining the Tóth fit results of CO_2 and N_2 adsorption obtained at 273 K it is possible to calculate adsorption selectivities using the IAST method. As a result of this calculation, the pressure dependent selectivities for samples carbonized between 600 °C and 1100 °C are plotted in Figure 9.

For the sample carbonized at 600 °C, the calculated IAST selectivity at 20 mbar is as high as 350. At higher pressures the selectivity drops and reaches saturation at 1 bar at a still very high value of 132, which is among the highest values reported for carbon materials in literature so far. When carbonized at higher temperatures, the carbon fibers exhibit a similar behavior for the IAST selectivity, but with lower values. For example, the IAST selectivity for a carbonization temperature of 700 °C at low pressures is as high as 250, while for 800 °C the sample shows a selectivity of 180 at the same pressure. The plateau values at ambient pressure equal high values of 130 and 80, respectively. In strong contrast to this, the samples carbonized at 1000 °C and 1100 °C exhibit IAST selectivities below 5.

The excellent adsorption selectivity towards CO_2 for carbonization temperatures of 600 °C and 700 °C, can be explained by a molecular sieve effect, which is schematically depicted in Figure 8. While CO_2 can penetrate the carbon interlayer spaces, N_2 molecules are excluded by their size, depending on the carbonization temperature of the adsorbent. In fact, the narrow ultramicropore volume – which is only accessible for CO_2 – shrinks for an increasing carbonization temperature, while the outer fiber surface – which is accessible for both gases – does not change significantly. Hence, the selectivity towards CO_2 decreases for an increasing carbonization temperature. Furthermore, the narrowest pores with a high adsorption selectivity are filled at comparatively low pressures due to the overlap of adsorption potentials of the pore walls, leading to an increase in adsorption energy which may be even enhanced by a selective interaction of nitrogen functional groups and CO_2. With increasing pressure, the rather unselective bare surface is covered, which results in a significantly higher selectivity for lower

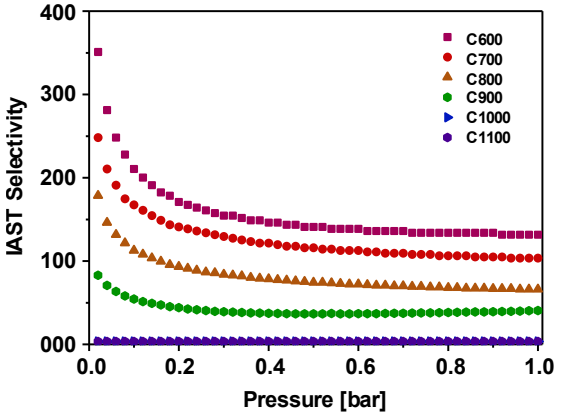

Figure 9: Pressure dependent IAST selectivity of CO_2 over N_2 (10:90) at 273K for electrospun, PAN derived carbon nanofibers prepared at carbonization temperatures from 600 °C to 1100 °C (C600 to C1100).

pressures. A similar trend for the pressure dependence of the IAST selectivity has been observed by Kim et al.[63], while Zhang et al.[64] and Wu et al.[65] found a contrary result of drastically increasing selectivity with higher pressures. For additional comparison, the selectivity values of previously reported carbons can be found in Table S3. However, none of the non-post-treated carbons reaches the extraordinarily high adsorption selectivity of the currently investigated carbons. The latter are only matched by tailor-made MOFs and very few post-treated carbons[21,66], which potentially enables the practical application of the electrospun CNFs in gas separation processes with relatively low CO_2 fraction feed gases.

Conclusion

In this work, the gas adsorption properties of PAN derived carbon nanofibers have been investigated. PAN fibers were prepared by electrospinning, crosslinking at 250 °C and carbonization at various temperatures ranging from 600 °C to 1100 °C. Within this temperature range three different temperature regimes influencing the gas adsorption properties have been identified. From 600 °C to 700 °C, the resulting carbon material can adsorb CO_2 and Ar in a high amount. However, the Ar adsorption appears to be very slow, due to kinetic hindrance. From 800 °C to 875 °C, the adsorption of CO_2 is still very high, while the Ar adsorption capacity decreases drastically. For a carbonization temperature of 900 °C and above, both CO_2 and Ar adsorption become very low, due to the significantly advancing carbonization of the investigated nanofibers. Based on micropore size distribution calculation, the gas adsorption properties of the carbon nanofibers are assumed to be highly dependent on the carbon layer distance, which is a function of the carbonization temperature and controls the access of gas molecules with different kinetic diameters such as Ar, N_2 and CO_2. Due to the narrow slit pore width provided by the carbon layer interspaces the CNFs, which were carbonized below 900 °C, offer superior low pressure CO_2 adsorption capabilities and extremely high IAST selectivities of up to 350. Furthermore, the influence of functional groups on the CO_2 adsorption properties was found to be less important than the carbon layer slit pores, which act as a molecular sieve for CO_2. A positive influence of the nitrogen functional groups was found as well. The molecular sieve effect and the interaction between functional groups and CO_2 make the PAN derived carbon nanofibers a promising material for gas adsorption and separation applications, especially for low pressures or diluted gas streams of CO_2 such as flue gas and might be tailored even further, beyond currently investigated gases and gas mixtures.

Experimental Section

Synthesis of CNFs

All chemicals were used as received without further purification. The carbon nanofibers were prepared by electrospinning of a solution containing 10 wt% Polyacrylonitrile (PAN) in Dimethylformamide (DMF). In a typical synthesis, 72 g of DMF (99.8%, VWR Chemicals, Germany) were added to 8 g of PAN (M_W = 150 000, BOC Science, USA). The mixture was stirred at ambient temperature for 3 days until a clear solution was obtained. In the following, the solution was electrospun in an electrospinning device equipped with a rotating drum collector (IME Medical Electrospinning, The Netherlands) at constant climate conditions of 25 °C and 30% relative humidity in a horizontal orientation. The solution was supplied by a syringe pump with a flow rate of 2.4 mL/h and pumped through a spinning needle of 0.8 mm inner diameter. The needle was moved laterally on an automated spinneret in a range of +/- 60 mm from the central position with a speed of 20 mm/s and a turn delay of 500 ms. The acceleration voltage was 25 kV and the needle-collector distance was 150 mm. The rotating drum collector had a diameter of 60 mm and a rotation speed of 1500 rpm. Electrospinning was performed for 6 hours with a corresponding solution volume of 14.4 mL.

After the electrospinning, the resulting PAN fiber mat was cut into pieces and dried in air for 1 hour at 150 °C. Then, the PAN polymer chains within the fibers were crosslinked in air at 250 °C for 15 hours. Subsequently, the fibers were carbonized for 3 hours in Argon atmosphere at constant temperatures ranging from 600 °C to 1100 °C. The heating rate of the tube furnace was 300 K/h, the cooling rate was 200 K/h.

Material Characterization

XPS measurements were performed on a Phi5000 VersaProbe II (ULVAC-Phi Inc., USA). For the individual measurements, monochromatic Al k-alpha radiation of 1.486 keV was applied. Peak analysis was performed using CasaXPS with a Shirley background as well as instrument specific corrections. The spectra were calibrated at the C1s signal to 284.4 eV.

For the elemental analysis a VarioelCube elemental analyzer (Elementar, Germany) was employed. 2 mg of each fiber sample were burned in CHN-mode and 10 mg in O-mode. In CHN mode, the samples were burned and the combustion products were separated and detected. In O mode the samples were treated in reductive atmosphere, where O containing fragments were converted to and detected as CO. This process was performed three times in both modes for each sample. For the sample which was carbonized at 900 °C polyethylene was added for better combustion.

Scanning Electron Microscopy (SEM) investigations were performed using a Quanta FEG 650 (FEI, USA). For each image, an acceleration voltage of 20 kV was used in combination with an Everhart-Thornley detector. For the measurements, small stripes of the samples were applied to the sample holder using a copper band for additional fixation and improved electrical conductivity.

Transmission Electron Microsopy (TEM) images were obtained using a Titan (FEI, USA). The samples were prepared by ultrasound mediated dispersion of the carbon fibers in ethanol.

Gas adsorption measurements were performed on an Autosorb iQ 2 (Quantachrome, USA), which was equipped with a cryocooler (CTI-cryogenics, USA). The samples were prepared by cutting the fiber mats into stripes of 1 mm by 5 mm, of which 50 – 100 mg were transferred into a glass sample tube. Subsequently, the samples were degassed for 8 hours under vacuum at 300 °C. For exact determination of the sample weight, the sample tubes were weighed three times in the empty state without sample. After loading with sample the degassing process was performed and the filled tubes were weighed again three times. From the difference of the average of both masses, the sample weight was determined.

Gas adsorption measurements were performed with Argon (5.2, Air Liquide, France) at 87 K for a general pore analysis. CO_2 (4.5, Air Liquide, France) adsorption measurements were performed at 273 K to investigate microporosity as well as to evaluate CO_2 adsorption energies and selectivities. The isotherms were evaluated regarding the surface area using the BET method[67]. Data evaluation according to the Dubinin-Radushkevich (DR) equation[57] was performed using the relative pressure range from 0.002 to 0.005 and a value of $\beta = 0.39$. The pore size distributions were obtained using the simulation methods provided by the measurement software Quantachrome ASiQWin® 5. For Ar at 87 K a QSDFT equilibrium model (quenched solid state density functional theory, Ar on carbon, slit pores) was used, whereas for CO_2 at 273 K an MC model (Monte Carlo, CO_2 on carbon, slit pores) was employed. Selectivity calculations according to the ideal adsorbed solution theory (IAST) were performed using the software 3Psim (3P instruments, Germany). Adsorption isotherms for N_2 (5.2, Air Liquide) were measured at 273 K. The resulting isotherms as well as the CO_2 adsorption isotherms were interpolated using a Toth isotherm model[68].

Acknowledgements

The authors acknowledge funding provided by the Deutsche Forschungsgemeinschaft (DFG, German Research Foundation) under Germany's Excellence Strategy – Cluster of Excellence 2186 "The Fuel Science Center" – ID: 390919832. The authors thank H. Hartmann (ZEA-3) and the Central Institute for Engineering, Electronics and Analytics (ZEA-3) of Forschungszentrum Jülich GmbH as a whole for performing the XPS measurements and data analysis and the CHNO analysis, respectively. Furthermore, the authors thank D. Kröger, Institute of Energy and Climate Research, Fundamental Electrochemistry (IEK-9) for performing the TEM measurements.

Keywords: carbon dioxide capture • carbon nanofibers • molecular sieve • carbon dioxide adsorption • ideal adsorbed solution theory

[1] R. K. Pachauri, L. Mayer (Eds.) *Climate change 2014: Synthesis report. Contribution of Working Groups I, II and III to the Fifth Assessment Report of the Intergovernmental Panel on Climate Change*, Intergovernmental Panel on Climate Change, Geneva, Switzerland, **2015**.
[2] J. Albo, M. Alvarez-Guerra, P. Castaño, A. Irabien, *Green Chem.* **2015**, *17*, 2304–2324.
[3] Q. Li, W. Zhu, J. Fu, H. Zhang, G. Wu, S. Sun, *Nano Energy* **2016**, *24*, 1–9.
[4] D. T. Whipple, P. J. A. Kenis, *J. Phys. Chem. Lett.* **2010**, *1*, 3451–3458.
[5] J. Wang, L. Huang, R. Yang, Z. Zhang, J. Wu, Y. Gao, Q. Wang, D. O'Hare, Z. Zhong, *Energy Environ. Sci.* **2014**, *7*, 3478–3518.
[6] Y. Liu, Z. U. Wang, H.-C. Zhou, *Greenhouse Gas Sci Technol* **2012**, *2*, 239–259.
[7] Z. Xiang, S. Leng, D. Cao, *J. Phys. Chem. C* **2012**, *116*, 10573–10579.
[8] B. Zheng, R. Yun, J. Bai, Z. Lu, L. Du, Y. Li, *Inorganic chemistry* **2013**, *52*, 2823–2829.
[9] F. Su, C. Lu, *Energy Environ. Sci.* **2012**, *5*, 9021.
[10] D. Ko, R. Siriwardane, L. T. Biegler, *Ind. Eng. Chem. Res.* **2003**, *42*, 339–348.
[11] M. R. Hudson, W. L. Queen, J. A. Mason, D. W. Fickel, R. F. Lobo, C. M. Brown, *Journal of the American Chemical Society* **2012**, *134*, 1970–1973.
[12] M. M. Lozinska, E. Mangano, J. P. S. Mowat, A. M. Shepherd, R. F. Howe, S. P. Thompson, J. E. Parker, S. Brandani, P. A. Wright, *Journal of the American Chemical Society* **2012**, *134*, 17628–17642.
[13] B. S. Caglayan, A. E. Aksoylu, *Journal of hazardous materials* **2013**, *252-253*, 19–28.
[14] M. S. Shafeeyan, W. M. A. W. Daud, A. Houshmand, A. Shamiri, *Journal of Analytical and Applied Pyrolysis* **2010**, *89*, 143–151.
[15] H. Zhao, X. Luo, H. Zhang, N. Sun, W. Wei, Y. Sun, *Greenhouse Gas Sci Technol* **2018**, *8*, 11–36.
[16] X.-q. Zhang, W.-c. Li, A.-H. Lu, *New Carbon Materials* **2015**, *30*, 481–501.
[17] N. A. Rashidi, S. Yusup, *Journal of CO2 Utilization* **2016**, *13*, 1–16.
[18] A.-H. Lu, S. Dai (Eds.) *Green chemistry and sustainable technology*, Springer, Heidelberg, **2014**.
[19] X. Xu, C. Song, J. M. Andresen, B. G. Miller, A. W. Scaroni, *Energy Fuels* **2002**, *16*, 1463–1469.
[20] S.-Y. Lee, S.-J. Park, *Journal of Industrial and Engineering Chemistry* **2015**, *23*, 1–11.
[21] M. Oschatz, M. Antonietti, *Energy Environ. Sci.* **2018**, *11*, 57–70.
[22] W. Xing, C. Liu, Z. Zhou, L. Zhang, J. Zhou, S. Zhuo, Z. Yan, H. Gao, G. Wang, S. Z. Qiao, *Energy Environ. Sci.* **2012**, *5*, 7323.
[23] D. Zabiegaj, M. Caccia, M. E. Casco, F. Ravera, J. Narciso, *Journal of CO2 Utilization* **2018**, *26*, 36–44.
[24] A. S. Ello, L. K.C. de Souza, A. Trokourey, M. Jaroniec, *Journal of CO2 Utilization* **2013**, *2*, 35–38.
[25] H. Wei, S. Deng, B. Hu, Z. Chen, B. Wang, J. Huang, G. Yu, *ChemSusChem* **2012**, *5*, 2354–2360.
[26] H. Cong, M. Zhang, Y. Chen, K. Chen, Y. Hao, Y. Zhao, L. Feng, *Carbon* **2015**, *92*, 297–304.
[27] J. Yu, M. Guo, F. Muhammad, A. Wang, F. Zhang, Q. Li, G. Zhu, *Carbon* **2014**, *69*, 502–514.
[28] Y. Li, B. Zou, C. Hu, M. Cao, *Carbon* **2016**, *99*, 79–89.
[29] X. Ren, H. Li, J. Chen, L. Wei, A. Modak, H. Yang, Q. Yang, *Carbon* **2017**, *114*, 473–481.
[30] S.-M. Hong, S. W. Choi, S. H. Kim, K. B. Lee, *Carbon* **2016**, *99*, 354–360.
[31] H.-Y. Hsiao, C.-M. Huang, M.-Y. Hsu, H. Chen, *Separation and Purification Technology* **2011**, *82*, 19–27.
[32] Z.-S. Hang, L.-H. Tan, X.-M. Cao, F.-Y. Ju, S.-J. Ying, F.-M. Xu, *Materials Letters* **2011**, *65*, 1079–1081.
[33] D. W. Kim, D. W. Jung, A. A. Adelodun, Y. M. Jo, *J. Appl. Polym. Sci.* **2017**, *134*, 45534.
[34] I. A. Principe, B. Murdoch, J. M. Flannigan, A. J. Fletcher, *Materials Today Chemistry* **2018**, *10*, 195–205.
[35] L. Li, X.-F. Wang, J.-J. Zhong, X. Qian, S.-L. Song, Y.-G. Zhang, D.-H. Li, *Ind. Eng. Chem. Res.* **2018**, *57*, 11608–11616.
[36] W. Shen, S. Zhang, Y. He, J. Li, W. Fan, *J. Mater. Chem.* **2011**, *21*, 14036.
[37] Y. Belmabkhout, V. Guillerm, M. Eddaoudi, *Chemical Engineering Journal* **2016**, *296*, 386–397.
[38] W. Travis, Dissertation, University College London, London, **2014**.
[39] M. Nandi, K. Okada, A. Dutta, A. Bhaumik, J. Maruyama, D. Derks, H. Uyama, *Chemical communications (Cambridge, England)* **2012**, *48*, 10283–10285.

[40] M. Gehring, H. Tempel, A. Merlen, R. Schierholz, R.-A. Eichel, H. Kungl, *RSC Adv.* **2019**, *9*, 27231–27241.
[41] A. Greiner, J. H. Wendorff, *Angewandte Chemie (International ed. in English)* **2007**, *46*, 5670–5703.
[42] M. Thommes, K. Kaneko, A. V. Neimark, J. P. Olivier, F. Rodriguez-Reinoso, J. Rouquerol, K. S.W. Sing, *Pure and Applied Chemistry* **2015**, *87*, 1051–1069.
[43] R. Schierholz, D. Kröger, H. Weinrich, M. Gehring, H. Tempel, H. Kungl, J. Mayer, R.-A. Eichel, *RSC Adv.* **2019**, *9*, 6267–6277.
[44] P. J. Goodhew, A. J. Clarke, J. E. Bailey, *Materials Science and Engineering* **1975**, *17*, 3–30.
[45] A. Kelly, J. N. Rabotnov (Eds.) *Handbook of composites*, */ series eds.: A. Kelly; Yu. N. Rabotnov ; Vol. 1,* 1. ed., 2. print ed., North-Holland, Amsterdam, **1988**, */ series eds.: A. Kelly; Yu. N. Rabotnov ; Vol. 1*.
[46] A. de PALMENAER, *Tekstil ve Mühendis* **2015**, *22*, 7–13.
[47] C.U. Pittman, W. Jiang, Z.R. Yue, C.A. Leon y Leon, *Carbon* **1999**, *37*, 85–96.
[48] C. U. Pittman, G.-R. He, B. Wu, S. D. Gardner, *Carbon* **1997**, *35*, 317–331.
[49] Z. Liu, Z. Du, H. Song, C. Wang, F. Subhan, W. Xing, Z. Yan, *Journal of Colloid and Interface Science* **2014**, *416*, 124–132.
[50] L. Laffont, M. Monthioux, V. Serin, R. B. Mathur, C. Guimon, M. F. Guimon, *Carbon* **2004**, *42*, 2485–2494.
[51] W. WATT, *Carbon* **1972**, *10*, 121–143.
[52] A. Vishnyakov, P. I. Ravikovitch, A. V. Neimark, *Langmuir : the ACS journal of surfaces and colloids* **1999**, *15*, 8736–8742.
[53] K. A. Cychosz, M. Thommes, *Engineering* **2018**, *4*, 559–566.
[54] K. S. W. Sing, R. T. Williams, *Part. Part. Syst. Charact.* **2004**, *21*, 71–79.
[55] M. K. Jain, A. S. Abhiraman, *J Mater Sci* **1987**, *22*, 278–300.
[56] A. F. Ismail, K. C. Khulbe, T. Matsuura, *Gas separation membranes. Polymeric and inorganic*, Springer, Cham, **2015**.
[57] S. Lowell, J. E. Shields, M. A. Thomas, M. Thommes, *Characterization of porous solids and powders. Surface area, pore size and density,* 1. reprint with some corr ed., Springer, Dordrecht, **2010**, *Vol. 16*.
[58] Z. Zhang, J. Zhou, W. Xing, Q. Xue, Z. Yan, S. Zhuo, S. Z. Qiao, *Physical chemistry chemical physics : PCCP* **2013**, *15*, 2523–2529.
[59] V. Presser, J. McDonough, S.-H. Yeon, Y. Gogotsi, *Energy Environ. Sci.* **2011**, *4*, 3059.
[60] T. Chen, S. Deng, B. Wang, J. Huang, Y. Wang, G. Yu, *RSC Adv.* **2015**, *5*, 48323–48330.
[61] X. Liu, C. Sun, H. Liu, W. H. Tan, W. Wang, C. Snape, *Chemical Engineering Journal* **2019**, *361*, 199–208.
[62] M. Yang, L. Guo, G. Hu, X. Hu, J. Chen, S. Shen, W. Dai, M. Fan, *Ind. Eng. Chem. Res.* **2016**, *55*, 757–765.
[63] Y. K. Kim, G. M. Kim, J. W. Lee, *J. Mater. Chem. A* **2015**, *3*, 10919–10927.
[64] S. Zhang, Q. Zhou, X. Jiang, L. Yao, W. Jiang, R. Xie, *Environmental technology* **2019**, 1–10.
[65] Y. Wu, J. Wang, Y. Muhammad, S. Subhan, Y. Zhang, Y. Ling, J. Li, Z. Zhao, Z. Zhao, *Chemical Engineering Journal* **2018**, *349*, 92–100.
[66] Q. Wang (Ed.) *Inorganic materials series*, Royal Society of Chemistry, Cambridge, **2018**.
[67] S. Brunauer, P. H. Emmett, E. Teller, *J. Am. Chem. Soc.* **1938**, *60*, 309–319.
[68] J. Tóth, *Acta Chi. Acad. Sci. Hung.* **1962**, *35*, 416